



## A novel calibration method for non-orthogonal shaft laser theodolite measurement system

Bin Wu, Fengting Yang, Wen Ding, and Ting Xue

Citation: *Review of Scientific Instruments* **87**, 035102 (2016); doi: 10.1063/1.4943017

View online: <http://dx.doi.org/10.1063/1.4943017>

View Table of Contents: <http://scitation.aip.org/content/aip/journal/rsi/87/3?ver=pdfcov>

Published by the AIP Publishing

---

### Articles you may be interested in

An innovative method for coordinate measuring machine one-dimensional self-calibration with simplified experimental process

*Rev. Sci. Instrum.* **84**, 055103 (2013); 10.1063/1.4801953

Calibration of measurement sensitivities of multiple micro-cantilever dynamic modes in atomic force microscopy using a contact detection method

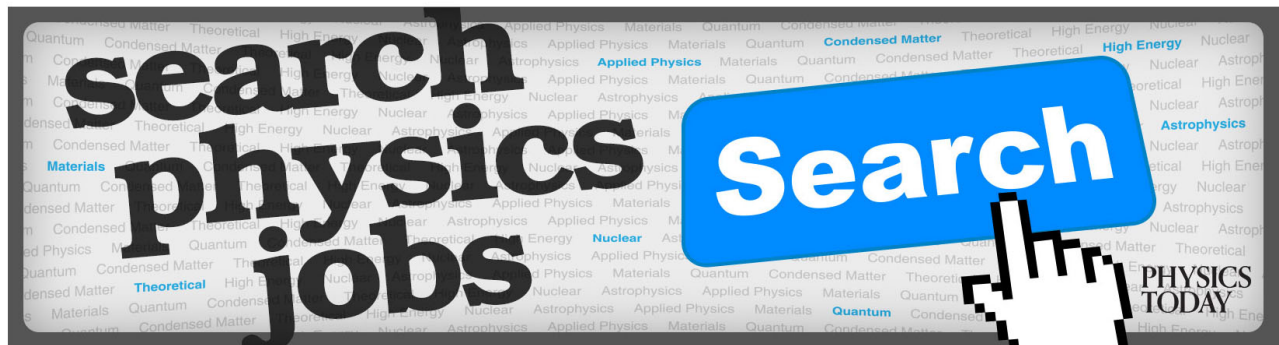
*Rev. Sci. Instrum.* **84**, 023703 (2013); 10.1063/1.4790194

Calibrating laser beam deflection systems for use in atomic force microscopes and cantilever sensors  
*Appl. Phys. Lett.* **88**, 083108 (2006); 10.1063/1.2177542

A fiber-optic attenuator calibration system using high frequency substitution method  
*Rev. Sci. Instrum.* **70**, 1603 (1999); 10.1063/1.1149639

Measurement of laser-induced acoustic waves with a calibrated optical transducer  
*J. Appl. Phys.* **82**, 1525 (1997); 10.1063/1.365953

---



# A novel calibration method for non-orthogonal shaft laser theodolite measurement system

Bin Wu,<sup>1,a)</sup> Fengting Yang,<sup>1</sup> Wen Ding,<sup>1</sup> and Ting Xue<sup>2,a)</sup>

<sup>1</sup>*State Key Laboratory of Precision Measuring Technology and Instruments, Tianjin University, Tianjin 300072, China*

<sup>2</sup>*College of Electrical Engineering and Automation, Tianjin Key Laboratory of Process Measurement and Control, Tianjin University, Tianjin 300072, China*

(Received 30 December 2015; accepted 11 February 2016; published online 3 March 2016)

Non-orthogonal shaft laser theodolite (N-theodolite) is a new kind of large-scale metrological instrument made up by two rotary tables and one collimated laser. There are three axes for an N-theodolite. According to naming conventions in traditional theodolite, rotary axes of two rotary tables are called as horizontal axis and vertical axis, respectively, and the collimated laser beam is named as sight axis. And the difference between N-theodolite and traditional theodolite is obvious, since the former one with no orthogonal and intersecting accuracy requirements. So the calibration method for traditional theodolite is no longer suitable for N-theodolite, while the calibration method applied currently is really complicated. Thus this paper introduces a novel calibration method for non-orthogonal shaft laser theodolite measurement system to simplify the procedure and to improve the calibration accuracy. A simple two-step process, calibration for intrinsic parameters and for extrinsic parameters, is proposed by the novel method. And experiments have shown its efficiency and accuracy. © 2016 AIP Publishing LLC. [<http://dx.doi.org/10.1063/1.4943017>]

## I. INTRODUCTION

Large-scale metrology has been widely applied to geological exploration, aviation and aerospace industry, shipbuilding, automotive and heavy equipment manufacturing, etc. Since definition of large-scale metrology was claimed by Purtrock in 1978,<sup>1</sup> a great number of scholars and manufacturers have spent decades in this field, and thousands of applications on large-scale metrology are developed.<sup>13</sup>

Industrial photogrammetry is one of the widely applied techniques.<sup>2–4</sup> However, to achieve a high-precision measurement, some co-targets have to be pasted on the objects to create measured features, which is a time-consuming process.

In addition, some other advanced large-scale metrological equipment, such as total station, laser tracker, and theodolite, is employed in different applications. Shi<sup>5</sup> used an electronic total station to measure control points and reference points for landslide dam deformation analysis. Summan<sup>6</sup> employed a Leica AT901B laser tracker to provide a high accuracy ground truth measurement for spatial calibration of large volume photogrammetry based metrology systems. Nubiola<sup>7</sup> used a laser tracker to calibrate an ABB IRB 1600 robot. And Wang built a vision guiding measurement system cooperated with two laser theodolites to satisfy the demand of shipbuilding.<sup>8</sup> Yet, all these precise instruments mentioned above, theodolite, laser tracker, and total station, rely on the orthogonality of their rotating shafts. The higher assembly accuracy they get, the better

performance they deliver. In recent years, iGPS (indoor global positioning system) or wMPS (workshop measuring positioning system) shows great potential for factory-wide deployment,<sup>9,10</sup> while it also has to work with high accurate reflectors.

In this case, a new kind of instrument called non-orthogonal shaft laser theodolite (N-theodolite) was introduced by Yang<sup>11</sup> recently. An N-theodolite can be made up of two rotary tables and one collimated laser conveniently. As in traditional theodolite, there are also three axes, but with no requirements on their orthogonality and intersection conditions. However, the calibration method proposed in Ref. 11 is really complicated, which need to measure both included angles between horizontal axis and vertical axis, and between horizontal axis and sight axis, not to mention those intricate trigonometric equations. In order to simplify the calibration procedure of N-theodolite, we propose a novel method of N-theodolite calibration, which can lead to a more simple operation and relevant performance.

This paper is organized as follows. Section II introduces the principle of N-theodolite measurement system, including the structure of a singular N-theodolite and the measurement system. Then Section III shows the derivation of the kinetic model of N-theodolite and its error analysis. Next the detailed calibration method of N-theodolite measurement system is presented in Section IV. Section V provides the simulation results based on Solidworks and Matlab and the measurement results from experimental setup in laboratory. Those experimental data validate the effectiveness of this method. Finally, a conclusion is drawn in Section VI.

<sup>a)</sup>Authors to whom correspondence should be addressed. Electronic addresses: wubin@tju.edu.cn and xueteng@tju.edu.cn

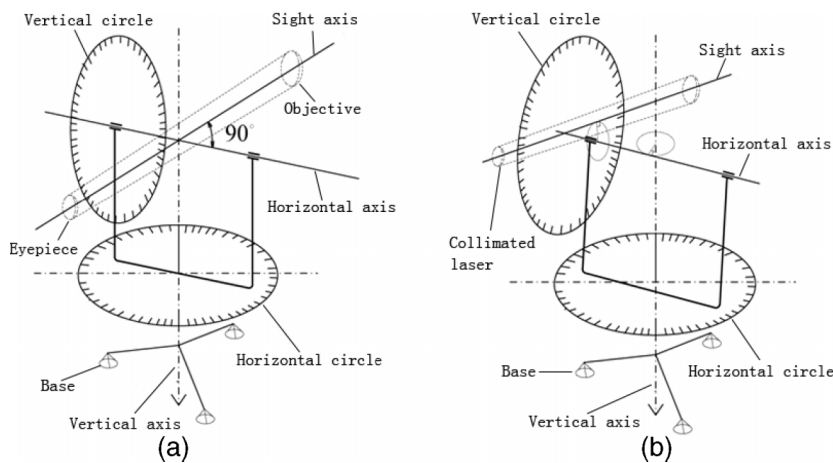


FIG. 1. Structure comparison between traditional theodolite and N-theodolite. (a) Orthogonal axes in traditional theodolite. (b) Non-orthogonal axes in N-theodolite.

## II. PRINCIPLE OF N-THEODOLITE MEASUREMENT SYSTEM

### A. Structure of N-theodolite

Non-orthogonal shaft laser theodolite is a new instrument with skewed shafts that differs from all traditional large-scale metrological equipments. Compared with traditional theodolite, N-theodolite has no strict requirements for the orthogonality and intersection conditions of its three rotating shafts. It means that an N-theodolite can be quickly and easily built up with separate rotary tables and a collimated laser. In addition, the collimated laser is introduced to substitute the optical lens of traditional theodolite. During measurement, the coincidence of the laser spots on the measured object denotes the intersection of the visualized sight axes. So combined with visual guiding technology, automatic measurement can be achieved based on N-theodolite. In analogy to traditional theodolite, we also name the three axes of N-theodolite which are the rotating axes of rotary tables and the location of collimated laser beam as “vertical axis,” “horizontal axis,” and “sight axis,” respectively, although it is no longer an accurate description. Fig. 1 shows the structure comparison between traditional theodolite and N-theodolite.

An N-theodolite prototype is shown in Fig. 2 and it is established by two rotary tables and one collimated laser. The three axes of N-theodolite are bifacial straights and the angle between any two axes is not 90°. In addition, two porcelain beads are pasted on the N-theodolite in order to fit out the intrinsic parameters, cooperating with a coordinate measuring machine (CMM). The details are shown in Section III A.

### B. N-theodolite measurement system

As with 3D coordinate measurement using traditional theodolite, an N-theodolite measuring system should consist of at least two N-theodolites. As shown in Fig. 3, when the left laser beam coincides with the right laser beam on a point of the measured object, the 3D coordinates of the point can be calculated based on the angles of rotation provided by the rotary tables of two N-theodolites and the mathematical measurement models.

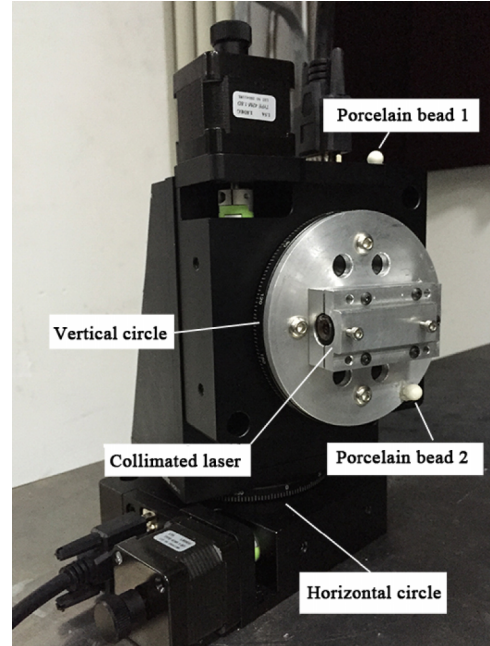


FIG. 2. N-theodolite prototype.

## III. MATHEMATICAL MODEL OF N-THEODOLITE MEASURING SYSTEM

### A. Intrinsic parameters of N-theodolite

Three axes of N-theodolite can be abstracted as three lines in 3D space. And the motion of sight axis, which is the key to get the coordinate of the measured point, could be divided into two kinds of motion, horizontal rotation and pitching rotation. Horizontal rotation is the rotating motion around vertical axis, and pitching rotation is the rotating motion around horizontal axis. To describe the movement of sight axis, we must give a description about the spatial pose of each axis which is the so-called intrinsic parameters. As seen in Fig. 4, every axis is described by a spatial point and a normalized direction vector. Thus there are 18 variables including three 3D coordinates for the fixed point in each axis and three 3D direction vectors for every axis to calibrate for a single N-theodolite.

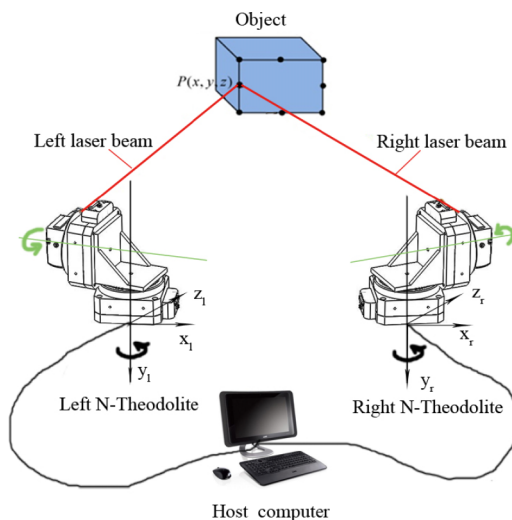


FIG. 3. Schematic diagram of N-theodolite measuring system.

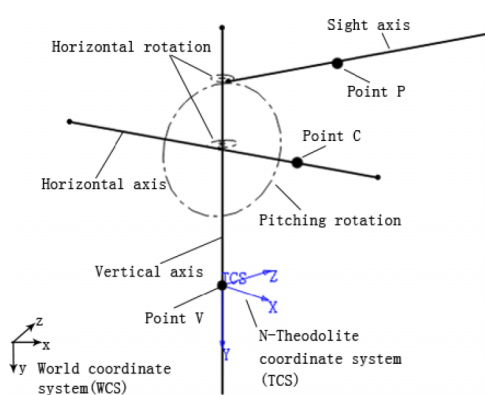


FIG. 4. The abstract structure of N-theodolite.

A CMM is employed to calibrate these intrinsic parameters of N-theodolite in the laboratory. Two accurate porcelain beads are pasted on the surfaces of two rotary tables, respectively (Figure 2). Rotating N-theodolite vertically and horizontally degree by degree and measuring the beads in each position by CMM, we are able to get the intrinsic parameters of horizontal axis and vertical axis by minimum-zone circle fitting from the trace of the beads. The circle center is chosen as the fixed point, and the normalized vector of the spatial circle is set as the direction vector. Then we block the laser beam in different places and measure the coordinate of the laser spots. The spatial pose of laser beam, equaling to the pose of sight axis, could be determined by linear fitting.

## B. N-theodolite kinetic model

CMM's measurement coordinate system is defined as the world coordinate system (WCS). As shown in Fig. 4, N-theodolite coordinate system (TCS) is the transformation of WCS. Translate WCS to the position where the origin point of WCS coincides with the chosen point V on vertical axis, usually the center of fitting circle of vertical axis finding process, and rotate WCS to make its y axis parallel to the vertical axis, and then TCS is established. Points C and P are

the fixed points on horizontal axis and sight axis we choose, respectively.

During measurement, the sight axis will rotate around the vertical axis for horizontal rotation and around the horizontal axis for pitching rotation. To simplify analysis, we consider horizontal rotation first, and then the pitching rotation.

Assume that  $H_{\text{original}}$  and  $H_{\text{dynamic}}$  are the initial and dynamic homogeneous direction vectors of horizontal axis, respectively, and  $R_{\text{hori}}$  is the rotation matrix between them, we have

$$H_{\text{dynamic}} = R_{\text{hori}} H_{\text{original}}. \quad (1)$$

Similarly, if we define that  $C_{\text{original}}$  is the original homogeneous coordinate vector of the fixed point C on horizontal axis and  $C_{\text{dynamic}}$  is its dynamic homogeneous coordinate vector, there is

$$C_{\text{dynamic}} = R_{\text{hori}} C_{\text{original}}, \quad (2)$$

where  $R_{\text{hori}} = \begin{bmatrix} \cos(\theta) & 0 & \sin(\theta) & 0 \\ 0 & 1 & 0 & 0 \\ -\sin(\theta) & 0 & \cos(\theta) & 0 \\ 0 & 0 & 0 & 1 \end{bmatrix}$  and  $\Theta$  is the horizontal rotation angle.

According to the structure of N-theodolite, rotation matrix  $R_{\text{hori}}$  also indicates the horizontal rotation of sight axis.

During pitching rotation, we notice that point C keeps constant position. So if  $V_{\text{original}}$  and  $V_{\text{dynamic}}$  represent the original and dynamic homogeneous direction vectors of sight axis, there is

$$V_{\text{dynamic}} = [q \circ [R_{\text{hori}} V_{\text{original}}] \circ \bar{q}]^{-1}, \quad (3)$$

where  $q$  is a quaternion indicating the rotation,  $q = \cos(\varphi/2) + \vec{h} \sin(\varphi/2)$ , where  $\varphi$  is the angle of pitching rotation. Symbols “[.]” and “[.]<sup>-1</sup>” indicate the transformation from homogeneous vector to quaternion and the inverse transform, respectively. Symbol “ $\circ$ ” means quaternion multiplication.

Similarly, if we define that  $P_{\text{original}}$  is the original homogeneous coordinate vector of chosen point P on the sight axis (collimated laser beam) and  $P_{\text{dynamic}}$  is its dynamic homogeneous coordinate vector, we have

$$P_{\text{dynamic}} = [q \circ [R_{\text{hori}} P_{\text{original}} - C_{\text{dynamic}}] \circ \bar{q} + [C_{\text{dynamic}}]]^{-1}. \quad (4)$$

The above equations denote the kinetic model of N-theodolite. Combining Eqs. (3) and (4), we can achieve the dynamic pose of sight axis. Based on the triangulation method, spatial coordinate of coincidence point of more than two sight axes can be determined.

## C. Error analysis for kinetic model

The actual measured value of point is formed by the sight axis which is described by a fixed point P and a homogeneous direction vector V. So calibration errors for point P and direction vector V determine the error of sight axis and kinetic model.

Since the kinetic error of sight axis is related to the kinetic error of horizontal axis, according to Eqs. (3) and (4), we are going to find out the variance of the elements of horizontal axis.

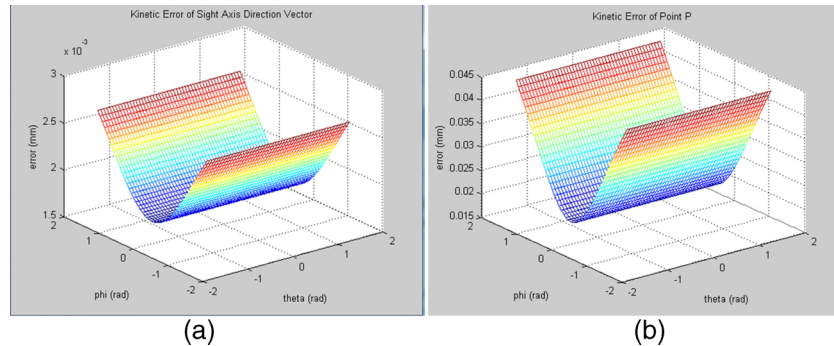


FIG. 5. The error distribution of sight axis. (a) Direction error of sight axis; (b) position error of sight axis.

For the kinetic model of N-theodolite, it is assumed that  $H_{dynamic} = [hx, hy, hz, 1]^T$  and  $\mathbf{h} = [hx, hy, hz]^T$ , meantime its residual calibration error is  $\mathbf{e}_{H_{dynamic}} = [e_x, e_y, e_z, e_\theta]^T$ , where  $e_x = e_y = e_z = 0.001$  mm and  $e_\theta = 0.005^\circ$  based on the measurement accuracy of CMM and movement accuracy of rotary tables used in N-theodolite prototype. Here we define an element-wise multiplication, for example,  $C = A \cdot * B$  means to multiply matrix A and B element by element and return the result in matrix C, just as the same process delivered by Matlab. The variance of  $H_{dynamic}$  can be expressed as

$$\Phi_{H_{dynamic}} = [\sigma_{hx}^2, \sigma_{hy}^2, \sigma_{hz}^2]^T = (J_{H_{dynamic}} \cdot * J_{H_{dynamic}})(\mathbf{e} \cdot * \mathbf{e}), \quad (5)$$

where  $J_{H_{dynamic}} = d\mathbf{h}/d\mathbf{x}$ , the Jacobian matrix of  $H_{dynamic}$ ,  $\mathbf{x} = [x, y, z, \theta]^T$ .

We encode all sources of errors and get

$$\begin{aligned} \Phi_{V_{dynamic}} &= [\sigma_\theta^2, \sigma_\varphi^2, \sigma_{hx}^2, \sigma_{hy}^2, \sigma_{hz}^2, \sigma_{vx}^2, \sigma_{vy}^2, \sigma_{vz}^2]^T, \\ \Phi_{P_{dynamic}} &= [\sigma_\theta^2, \sigma_\varphi^2, \sigma_{hx}^2, \sigma_{hy}^2, \sigma_{hz}^2, \sigma_{px}^2, \sigma_{py}^2, \sigma_{pz}^2, \sigma_{cx}^2, \sigma_{cy}^2, \sigma_{cz}^2]^T, \end{aligned} \quad (6)$$

where  $\sigma_\theta^2 = \sigma_\varphi^2 = (0.005\pi/180)^2$ , determined by the rotating accuracy of rotary table.  $\sigma_{vx}^2 = \sigma_{vy}^2 = \sigma_{vz}^2 = \sigma_{px}^2 = \sigma_{py}^2 = \sigma_{pz}^2 = \sigma_{cx}^2 = \sigma_{cy}^2 = \sigma_{cz}^2 = 0.001^2$  mm<sup>2</sup>, determined by the coordinate calibrating accuracy of CMM. Therefore the two elements of pose error of sight axis can be described as follows:

$$E_{V_{dynamic}} = \sqrt{\|(J_{V_{dynamic}} \cdot * J_{V_{dynamic}})\Phi_{V_{dynamic}}\|_1}, \quad (8)$$

$$E_{P_{dynamic}} = \sqrt{\|(J_{P_{dynamic}} \cdot * J_{P_{dynamic}})\Phi_{P_{dynamic}}\|_1}, \quad (9)$$

where  $E_{V_{dynamic}}$  is the direction error of sight axis and  $E_{P_{dynamic}}$  is the position error of sight axis.  $J_{V_{dynamic}}$  refers to the Jacobian matrix of  $V_{dynamic}$ , and  $J_{P_{dynamic}}$  refers to the Jacobian matrix of  $P_{dynamic}$ . The error distribution is shown in Fig. 5.

It is a reasonable result, since we set horizontal rotation angle  $\theta = 0$  and pitch angle  $\varphi = 0$  in the position where the sight axis is parallel with the z-axis during the calculation. In other words, this is the gesture we calibrate with CMM. So the position where  $\varphi = 0$  should be the most accurate place, the only residual there caused by the calibrating error of CMM. The more it rotates the more error it delivers. Additionally, we have normalized the direction vector of sight axis, so the direction error of sight axis is significantly lower than the position error of it numerically.

As shown in Fig. 5, we can find that the variation of errors is very small when pitch angle remains constant and the horizontal rotation angle changes. On the contrary, there is a large variation of errors. So during measurement, the kinetic error caused by horizontal rotation can be ignored, but the kinetic error caused by pitching rotation should be considered sufficiently. In practice, we adjust the gesture of N-theodolite to aim at the middle part of the whole measured object after initialization ( $\theta = 0$  and  $\varphi = 0$ ) before calibration and measurement process. And it is essential to put the scale bar at the area near that part during the whole calibration process.

#### IV. CALIBRATION OF N-THEODOLITE MEASURING SYSTEM

To achieve 3D measurement, the measuring system needs at least two N-theodolites, and the relationship of these N-theodolites should be calibrated precisely in advance. The relationship of these N-theodolites is called as system parameters or extrinsic parameters which include a rotation matrix R and a translation vector T. To calibrate these extrinsic parameters, a scale bar is placed at several different positions inside the measurement space, and both N-theodolites aim the targets on the scale bar manually. As shown in Fig. 6, the solid lines indicate pointing at the left target of scale bar and the dashed lines illustrate aiming to the right target.

In practice, to aim the target accurately, we rotate one N-theodolite to aim the target first and then remove the laser spot to the next target when the other N-theodolite aims the same target. The aiming condition is judged manually, see Fig. 7.

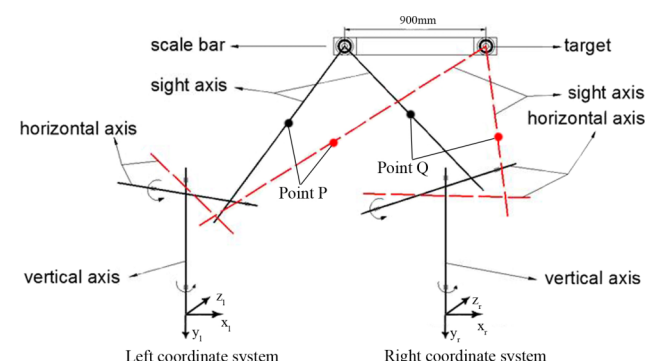


FIG. 6. Intersection of two N-theodolites.



FIG. 7. Aiming condition.

And Eq. (10) indicates the correlation which transforms the TCS of right N-theodolite to left N-theodolite's TCS. We can get one equation at each time the sight axes intersect at a target,

$$\begin{bmatrix} \lambda V_{dynamic\_l} + P_{dynamic} \\ 1 \end{bmatrix} = \begin{bmatrix} R & T \\ 0 & 1 \end{bmatrix} \begin{bmatrix} k V_{dynamic\_r} + Q_{dynamic} \\ 1 \end{bmatrix}, \quad (10)$$

where  $R = \begin{bmatrix} r_1 & r_2 & r_3 \\ r_4 & r_5 & r_6 \\ r_7 & r_8 & r_9 \end{bmatrix}$ ,  $T = [t_x \ t_y \ t_z]^T$ , normalized the direction vector of sight axis of left N-theodolite  $V_{dynamic\_l} = [V_{lx}, V_{ly}, V_{lz}]^T$ , and the chosen point on sight axis of left N-theodolite  $P_{dynamic} = [P_x, P_y, P_z]^T$ , while  $V_{dynamic\_r} = [V_{rx}, V_{ry}, V_{rz}]^T$  and  $Q_{dynamic} = [Q_x, Q_y, Q_z]^T$  are the corresponding right ones.  $\lambda$  and  $k$  are scale factors. So we have

$$f = (V_{lx}A_2 - V_{ly}A_1)(V_{lx}B_1 - V_{ly}B_3) - (V_{lx}A_3 - V_{ly}A_1)(V_{lx}B_1 - V_{lx}B_2) = 0, \quad (11)$$

where

$$\begin{cases} A_1 = r_1V_{rx} + r_2V_{ry} + r_3V_{rz} \\ A_2 = r_4V_{rx} + r_5V_{ry} + r_6V_{rz} \\ A_3 = r_7V_{rx} + r_8V_{ry} + r_9V_{rz} \\ B_1 = r_1Q_x + r_2Q_y + r_3Q_z + t_x - P_x \\ B_2 = r_4Q_x + r_5Q_y + r_6Q_z + t_y - P_y \\ B_3 = r_7Q_x + r_8Q_y + r_9Q_z + t_z - P_z \end{cases}$$

According to the orthogonality of  $R$ , which is denoted by Eq. (12), once we get more than six intersections, we could figure out the matrices  $R$  and  $T$  by

$$\begin{cases} g_1(x) = r_1^2 + r_2^2 + r_3^2 - 1 \\ g_2(x) = r_4^2 + r_5^2 + r_6^2 - 1 \\ g_3(x) = r_7^2 + r_8^2 + r_9^2 - 1 \\ g_4(x) = r_1r_4 + r_2r_5 + r_3r_6 \\ g_5(x) = r_1r_7 + r_2r_8 + r_3r_9 \\ g_6(x) = r_4r_7 + r_5r_8 + r_6r_9 \end{cases}, \quad (12)$$

$$F_i(x) = f_i^2(x) + \sum_{j=1}^n \sigma_j g_j^2(x) \rightarrow 0, n = 6, \quad (13)$$

where  $\sigma_j$  are penalty factors for constraints and they are all set as 3 in this paper. And Levenberg-Marquardt algorithm is employed to solve this problem.

However, there exist some additional errors like gross error and random error during the process. To refine the calibration, a further step is adopted.

From Eq. (12), we could get a rough value of  $R$  and  $T$ , so the midpoint coordinate of common perpendicular of two sight axes can be calculated when they “intersect” at the target of a scale bar. The quotation marks here mean the fact that, in most cases, they do not really or totally intersect. Then we set  $L$  as

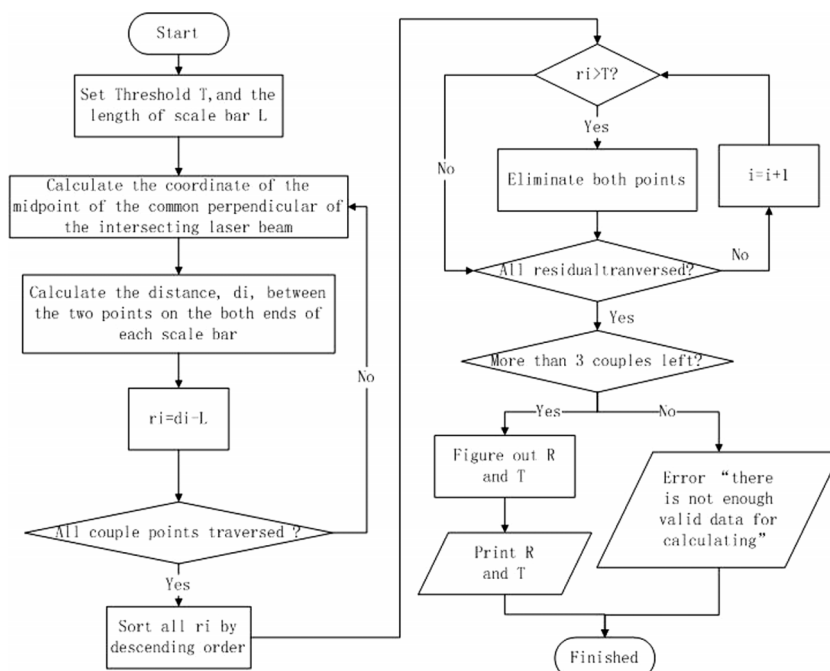


FIG. 8. Flow chart of precisely system parameters calculation.

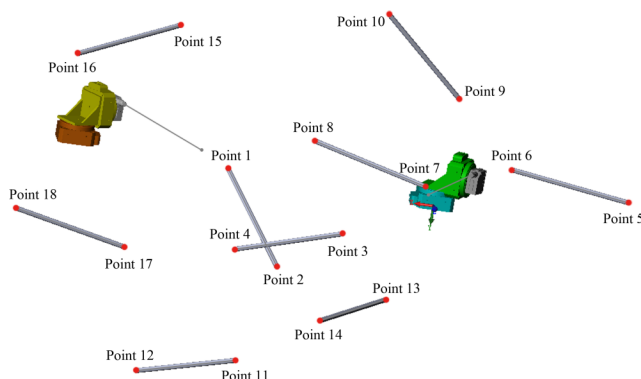


FIG. 9. Schematic diagram of simulation platform.

the length of scale bar. During the calibration,  $L$  is invariant and equals to the distance between the two intersection points of the same bar. If  $T_1(X_1, Y_1, Z_1)$  and  $T_2(X_2, Y_2, Z_2)$  denote the two intersection points, we have the residual value,

$$r_i = \sqrt{(X_{i1} - X_{i2})^2 + (Y_{i1} - Y_{i2})^2 + (Z_{i1} - Z_{i2})^2} - L. \quad (14)$$

Once the residual value was greater than the threshold value set in advance, both points would be eliminated. At last, if more than 3 couples of data are preserved, we set all of them validated and add all  $r_i$  functions into Eq. (13) as constraint conditions to refine  $R$  and  $T$ . The flow chart of this process is shown as Fig. 8.

## V. EXPERIMENTS OF N-THEODOLITE SYSTEM CALIBRATION

### A. Simulation of N-theodolite system calibration

Based on Solidworks and Matlab, we set up a simulation platform for N-theodolite measuring system shown in Fig. 9. Several scale bars with 900 mm length are placed in different positions in the measurement space. There are two target points on the ends of each scale bar. Two N-theodolite models aim at these points at a same time. 8 points are chosen to calibrate the extrinsic parameters of the N-theodolite measuring system. The remaining points are used for validation of the calibration method. The measurement space for simulation is 6700 mm  $\times$  4100 mm  $\times$  4000 mm. Intrinsic parameters of two simulated N-theodolites are shown in Table I.

Based on calibration method and the chosen 8 points, we got the extrinsic parameters of the N-theodolite measuring system as follows:

$$R = \begin{bmatrix} 0.9730 & 0.2241 & -0.0554 \\ -0.2267 & 0.9729 & -0.0452 \\ 0.0438 & 0.0566 & 0.9974 \end{bmatrix},$$

$$T = \begin{bmatrix} 5093.0175 \\ -377.6231 \\ 284.7634 \end{bmatrix}.$$

TABLE I. Intrinsic parameters of two N-theodolites generated from 3D models (mm).

	Left N-theodolite	Right N-theodolite
Vertical axis	Vector (0.0000, -1.0000, 0.0000) Point (0.0000, 0.0000, 0.0000)	Vector (0.0000, -1.0000, 0.0000) Point (0.0000, 0.0000, 0.0000)
Horizontal axis	Vector (-0.9848, -0.1736, 0.0000) Point (-226.3740, -872.3880, 0.0000)	Vector (-0.9848, -0.1736, 0.0000) Point (231.2980, -873.2570, 0.0000)
Sight axis	Vector (0.0000, 0.0000, -1.0000) Point (-224.4910, -883.0710, 16.8030)	Vector (0.0000, 0.0000, -1.0000) Point (-229.4150, -883.9390, 16.8030)

TABLE II. Comparison between measured value and truth value (mm).

No.	Measured value	Truth value	Deviation
1	1866.175, 227.488, 2681.276	1866.181, 227.547, 2681.283	0.058
2	2642.353, 27.847, 2271.783	2642.346, 27.911, 2271.755	0.070
3	1154.871, 327.406, 2526.264	1154.868, 327.472, 2526.247	0.068
4	2044.207, 381.742, 2399.363	2044.215, 381.778, 2399.310	0.065
5	-2636.854, -840.998, 2614.898	-2636.998, -840.931, 2615.029	0.206
6	-1737.008, -840.978, 2615.037	-1736.998, -840.931, 2615.029	0.049
7	185.022, -680.175, 2314.275	185.032, -680.128, 2314.229	0.067
8	1085.052, -680.183, 2314.291	1085.032, -680.128, 2314.229	0.085
9	365.138, -1636.600, 3185.758	365.104, -1636.532, 3185.671	0.116
10	1168.431, -2030.001, 3285.456	1168.409, -2029.927, 3285.379	0.109
11	2197.765, 1640.079, 4036.369	2197.774, 1640.075, 4036.364	0.011
12	3005.747, 1849.758, 3699.958	3005.761, 1849.804, 3699.955	0.048
13	126.950, 989.149, 2178.239	126.945, 989.221, 2178.261	0.076
14	982.923, 1224.546, 2326.114	982.949, 1224.594, 2326.099	0.057
15	2928.477, -2254.125, 2822.550	2928.406, -2254.083, 2822.512	0.091
16	3809.991, -2105.308, 2926.265	3809.935, -2105.256, 2926.229	0.085
17	3378.892, -79.5413, 2904.984	3378.804, -79.464, 2905.110	0.172
18	4263.831, -194.163, 3021.857	4263.811, -194.11, 3021.812	0.072

TABLE III. Intrinsic parameters of N-theodolites calibrated by CMM (mm).

	Left N-theodolite	Right N-theodolite
Vertical axis	Vector (0.0003, -0.0005, 1.0000) Point (301.9591, 291.4374, -535.8080)	Vector (-0.0004, 0.0029, 1.0000) Point (301.1068, 293.5497, -534.8184)
Horizontal axis	Vector (0.0225, 0.9997, -0.0009) Point (310.1742, 189.1041, -613.1614)	Vector (0.0013, 1.0000, -0.0034) Point (314.4189, 189.5606, -612.1547)
Sight axis	Vector (-0.9973, 0.0294, 0.0672) Point (310.3943, 181.0313, -612.7528)	Vector (-0.9764, 0.0000, 0.2161) Point (314.1608, 183.2550, -612.5652)

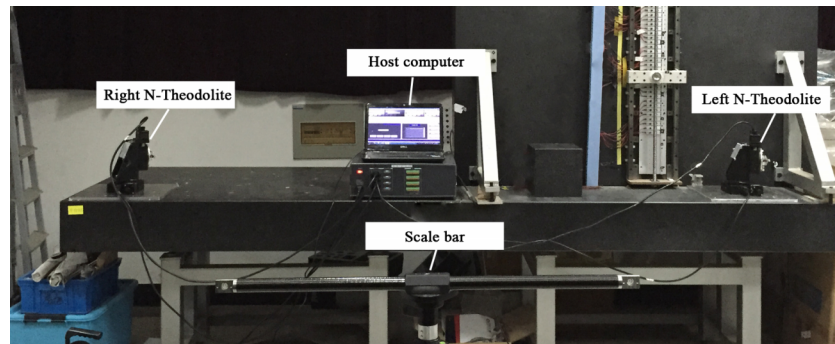


FIG. 10. Experiment condition.

TABLE IV. Measured lengths of a 900.081-mm scale bar.

Point no.	Left/right	Horizontal angle (deg)	Vertical angle (deg)	Measured length (mm)	Deviation (mm)
1	Left	114.810	-1.320	900.034	-0.047
	Right	55.725	-10.370		
2	Left	130.975	-2.005	900.085	0.004
	Right	74.77	-10.245		
3	Left	110.055	-5.620	900.047	-0.034
	Right	52.915	-13.965		
4	Left	128.770	-5.865	900.168	0.087
	Right	69.935	-14.855		
5	Left	117.175	-4.415	900.179	0.098
	Right	45.555	-12.970		
6	Left	134.615	-5.0150	899.965	-0.116
	Right	66.320	-13.930		
7	Left	112.960	-3.760	900.017	-0.064
	Right	46.215	-12.485		
8	Left	134.245	-3.955	73.615	-15.560
	Right	63.480	-12.645		
9	Left	111.855	-4.710	125.755	1.735
	Right	44.010	-12.950		
10	Left	132.435	-4.775	86.670	-5.375
	Right	62.200	-13.250		
11	Left	113.900	1.815	106.060	-7.370
	Right	70.635	-6.555		
12	Left	125.755	1.735	57.555	-15.265
	Right	86.670	-5.375		
13	Left	121.345	-6.885	73.615	-15.560
	Right	73.615	-15.560		

Using the simulated intrinsic parameters and the calibrated extrinsic parameters of the N-theodolite measuring system, we obtained 3D coordinates of the remaining 18 points. The measured and truth 3D coordinates which are generated by Solidworks and their deviation are shown in Table II.

Combining Fig. 9 and Table II, it is safe to conclude that high precision measurement can be achieved in the center area of the measuring system, which is similar to the traditional theodolite measurement system does.<sup>12</sup> And the measurement system is able to deliver a high performance, whose measurement accuracy in center area is better than 0.1 mm in such a large measured space, cooperating with the novel calibration method proposed in this paper.<sup>14–28</sup>

## B. Experiment of N-theodolite system calibration

In the experiment, we employed a CMM to calibrate the intrinsic parameters. By detecting the small pasted balls rotating around the corresponding axes, we can find out the horizontal and vertical axes by circle fitting. And the spatial position of sight axis could be figured out after shooting the ruby probe of CMM in different positions with horizontal and vertical angles of N-theodolite fixed. The intrinsic parameters under the CMM coordinate system (WCS) are shown in Table III.

Using the algorithm mentioned above, we place a length fixed scale bar (900.081 mm) in 4 different places to figure out the position relation matrix between left N-theodolite and right N-theodolite,

$$R = \begin{bmatrix} 0.999\,55 & -0.002\,174\,9 & -0.030\,014 \\ 0.002\,102\,1 & 0.999\,99 & -0.002\,466\,8 \\ 0.030\,020 & 0.002\,400\,9 & 0.999\,55 \end{bmatrix},$$

$$T = \begin{bmatrix} 2598.1707 \\ 75.1923 \\ 6.9396 \end{bmatrix}.$$

Because of the difficulty to obtain an extremely high accurate spatial coordinate in laboratory, we turn to compare the measured value with the real lengths of the scale bar (900.081 mm) to evaluate the accuracy of the measuring system. The scale bar is placed in 7 places more, measured by N-theodolite system, as Figure 10 shows. And the results are shown in Table IV.

From the comparison, we can approve that the measuring accuracy of N-theodolite calibrated by the new method is better than 0.12 mm in the real experimental application.

## VI. CONCLUSION

In this paper, a novel method of N-theodolite calibration is proposed. Despite the uncertainty of assemblage, the calibration process could be simply divided into two steps, calibrating intrinsic parameters by a CMM and calibrating the relative position between two N-theodolites using a scale bar. A kinetic model of N-theodolite is also proposed to obtain the precise dynamic pose of sight axis to calculate the

coordinate of targets correctly. Euler angle and quaternion are employed in the algorithm of the novel calibration method whose accuracy is approved by the simulation and experiment.

## ACKNOWLEDGMENTS

This work was funded by the National Natural Science Foundation of China (No. 51475328).

- <sup>1</sup>M. J. Puttock, "Large-Scale Metrology," *CIRP Ann.* **27**(1), 351–356 (1978).
- <sup>2</sup>Y. Shang, Q. Yu, Z. Yang, Z. Xu, and X. Zhang, "Displacement and deformation measurement for large structures by camera network," *Opt. Lasers Eng.* **54**, 247–254 (2014).
- <sup>3</sup>F. Franceschini, M. Galetto, and G. Genta, "Multivariate control charts for monitoring internal camera parameters in digital photogrammetry for LSDM (Large-Scale Dimensional Metrology) applications," *Precis. Eng.* **42**, 133–142 (2015).
- <sup>4</sup>Z. Xiao, J. Liang, D. Yu, and A. Asundi, "Large field-of-view deformation measurement for transmission tower based on close-range photogrammetry," *Measurement* **44**(9), 1705–1712 (2011).
- <sup>5</sup>Z.-M. Shi, Y.-Q. Wang, M. Peng, S.-G. Guan, and J.-F. Chen, "Landslide dam deformation analysis under aftershocks using large-scale shaking table tests measured by videogrammetric technique," *Eng. Geol.* **186**, 68–78 (2015).
- <sup>6</sup>R. Summan, S. G. Pierce, C. N. Macleod, G. Dobie, T. Gears, W. Lester, P. Pritchett, and P. Smyth, "Spatial calibration of large volume photogrammetry based metrology systems," *Measurement* **68**, 189–200 (2015).
- <sup>7</sup>A. Nubiola and I. A. Bonev, "Absolute calibration of an ABB IRB 1600 robot using a laser tracker," *Rob. Comput. Integr. Manuf.* **29**(1), 236–245 (2013).
- <sup>8</sup>B. Wu and B. Wang, "Automatic measurement in large-scale space with the laser theodolite and vision guiding technology," *Adv. Mech. Eng.* **2013**, 629385, available online at <http://ade.sagepub.com/content/5/629385.full.pdf+html>.
- <sup>9</sup>A. R. Norman, A. Schönberg, I. A. Gorlach, and R. Schmitt, "Validation of iGPS as an external measurement system for cooperative robot positioning," *Int. J. Adv. Manuf. Technol.* **64**(1–4), 427–446 (2013).
- <sup>10</sup>Z. Xiong, J. G. Zhu, Z. Y. Zhao, X. Y. Yang, and S. H. Ye, "Workspace measuring and positioning system based on rotating laser planes," *Mechanics* **18**(1), 94–98 (2012).
- <sup>11</sup>B. Wu and S. Yang, "Research of measurement technology of non-orthogonal shaft laser theodolites," *Laser Technol.* **39**(5), 603–609 (2015).
- <sup>12</sup>H. Hong-lu and W. Wei, "Multi-photoelectric theodolite deployment optimization of intersection measurement," in *4th IEEE Conference on Industrial Electronics and Applications, ICIEA 2009* (IEEE, 2009), pp. 4021–4026.
- <sup>13</sup>F. Franceschini, M. Galetto, D. Maisano, and L. Mastrogiovanni, "Large-scale dimensional metrology (LSDM): From tapes and theodolites to multi-sensor systems," *Int. J. Precis. Eng. Manuf.* **15**(8), 1739–1758 (2014).
- <sup>14</sup>B. P. Ickes, "A new method for performing digital control system attitude computations using quaternions," *AIAA J.* **8**(1), 13–17 (1970).
- <sup>15</sup>H. C. Longuet-Higgins, "A computer algorithm for reconstructing a scene from two projections," *Nature* **293**(5828), 133–135 (1981).
- <sup>16</sup>J. B. Kuipers, *Quaternions and Rotation Sequences* (Princeton University Press, Princeton, 1999), Vol. 66.
- <sup>17</sup>S. Yin, Y. Ren, Y. Guo, J. Zhu, S. Yang, and S. Ye, "Development and calibration of an integrated 3D scanning system for high-accuracy large-scale metrology," *Measurement* **54**, 65–76 (2014).
- <sup>18</sup>L. Ma, T. Cao, J. Wang, and A. Sun, "Discussion on inspecting the assembling components by using large volume metrology instruments," *Metrol. Meas. Technol.* **2**, 003 (2013).
- <sup>19</sup>J. J. Moré, "The Levenberg-Marquardt algorithm: Implementation and theory," in *Numerical Analysis* (Springer, Berlin, Heidelberg, 1978), pp. 105–116.
- <sup>20</sup>S. De Ma, "A self-calibration technique for active vision systems," *IEEE Trans. Rob. Autom.* **12**(1), 114–120 (1996).
- <sup>21</sup>A. Björck, *Numerical Methods for Least Squares Problems* (Siam, 1996).
- <sup>22</sup>A. B. Forbes, B. Hughes, and W. Sun, "Comparison of measurements in co-ordinate metrology," *Measurement* **42**(10), 1473–1477 (2009).
- <sup>23</sup>L. Hinsken, "A singularity-free algorithm for spatial orientation of bundles," *Int. Arch. Photogramm. Remote Sens.* **27**(B5), 262–272 (1988).

- <sup>24</sup>M. Ferrucci, B. Muralikrishnan, D. Sawyer, S. Phillips, P. Petrov, Y. Yakovlev, A. Astrelin, S. Milligan, and J. Palmateer, "Evaluation of a laser scanner for large volume coordinate metrology: A comparison of results before and after factory calibration," *Meas. Sci. Technol.* **25**(10), 105010 (2014).
- <sup>25</sup>M. Galetto, L. Mastrogiacomo, D. Maisano, and F. Franceschini, "Cooperative fusion of distributed multi-sensor LVM (Large Volume Metrology) systems," *CIRP Ann. Manuf. Technol.* **64**(1), 483–486 (2015).
- <sup>26</sup>O. D. Faugeras and S. Maybank, "Motion from point matches: Multiplicity of solutions," *Int. J. Comput. Vision* **4**(3), 225–246 (1990).
- <sup>27</sup>S.-H. Suh, E.-S. Lee, and Se-Y. Jung, "Error modelling and measurement for the rotary table of five-axis machine tools," *Int. J. Adv. Manuf. Technol.* **14**(9), 656–663 (1998).
- <sup>28</sup>V. Zarikas, V. Gikas, and C. P. Kitsos, "Evaluation of the optimal design 'cosinor model' for enhancing the potential of robotic theodolite kinematic observations," *Measurement* **43**(10), 416–1424 (2010).